

Reduced-Order Simulation of Flexible Meta-Materials

Kurt Leimer

Technische Universität Wien (TU Wien)

Przemyslaw Musialski

New Jersey Institute of Technology (NJIT)

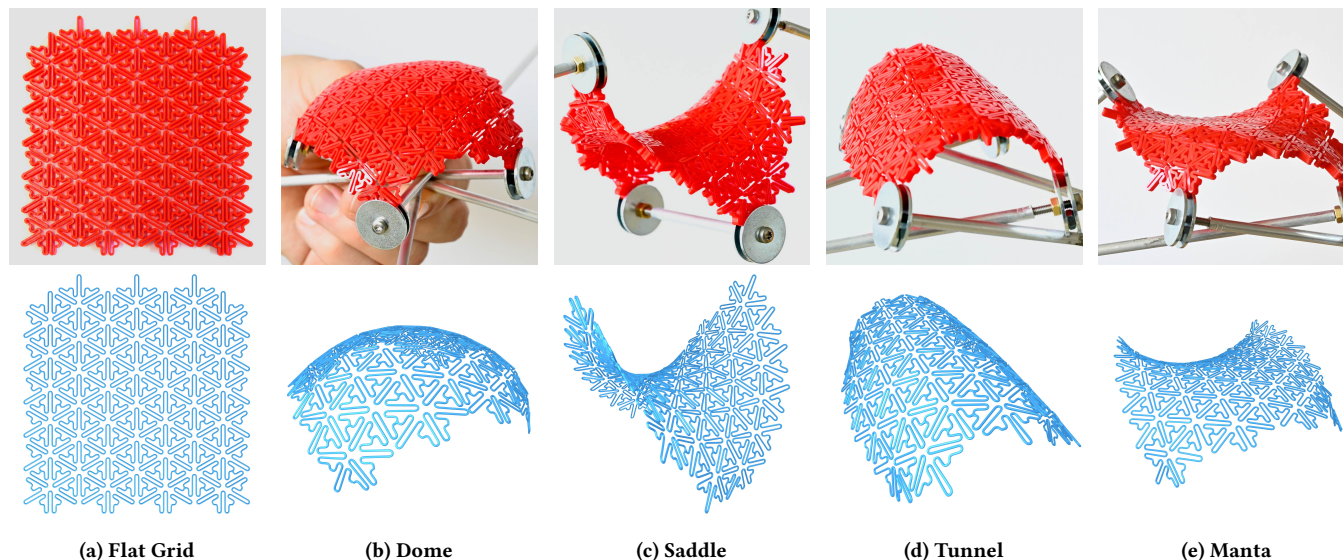


Figure 1: Patterns made from rigid material can be made flexible by introducing meso-structures. Top: 3d-printed pattern deformed into various shapes. Bottom: Simulation of pattern with similar structure.

ABSTRACT

We propose a reduced-order simulation and optimization technique for a type of digital materials which we denote as geometric meta-materials. They are planar cellular structures, which can be fabricated in 2d and folded in 3d space and thus well shaped into sophisticated 3d surfaces. They obtain their elasticity attributes mainly from the geometry of their cellular elements and their connections. While the physical properties of the base material (i.e., the physical substance) of course influence the behavior as well, our goal is to factor them out. However, the simulation of such complex structures still comes with a high computational cost. We propose an approach to reduce this computational cost by abstracting the meso-structures and encoding the properties of their elastic deformation behavior into a different set of material parameters. We can thus obtain an approximation of the deformed pattern by simulating a simplified version of the pattern using the computed material parameters.

CCS CONCEPTS

• **Computing methodologies** → *Shape modeling*.

KEYWORDS

computational design, fabrication, elastic deformation, meso-structures, meta-materials

ACM Reference Format:

Kurt Leimer and Przemyslaw Musialski. 2020. Reduced-Order Simulation of Flexible Meta-Materials. In *Symposium on Computational Fabrication (SCF '20)*, November 5–6, 2020, Virtual Event, USA. ACM, New York, NY, USA, 11 pages. <https://doi.org/10.1145/3424630.3425411>

1 INTRODUCTION

In the field of computational design of meta-materials, complex patterns of meso-structures have seen increased interest because of the ability to locally control their flexibility through adjustment of the meso-structure parameters. Such structures come with a number of advantages like, despite the simplicity of their fabrication, their ability to nestle to sophisticated free-form surfaces. We can think of such materials as meshes composed of nodes that are connected by edges of complex geometry. Additionally, these meshes are not flat, but have a certain thickness (cf. Fig. 1).

The assumption is that mechanical properties of such structures can be homogenized [Panetta et al. 2015], i.e., the way how the structure stretches, bends, deforms, or breaks, depend continuously on the interplay of individual connections, their thickness and size, and their angular deflections about nodes. If such a structure is exposed to internal and external loads, the forces spread across the

Permission to make digital or hard copies of all or part of this work for personal or classroom use is granted without fee provided that copies are not made or distributed for profit or commercial advantage and that copies bear this notice and the full citation on the first page. Copyrights for components of this work owned by others than ACM must be honored. Abstracting with credit is permitted. To copy otherwise, or republish, to post on servers or to redistribute to lists, requires prior specific permission and/or a fee. Request permissions from permissions@acm.org.

SCF '20, November 5–6, 2020, Virtual Event, USA

© 2020 Association for Computing Machinery.

ACM ISBN 978-1-4503-8170-3/20/11...\$15.00

<https://doi.org/10.1145/3424630.3425411>

elements and stress individual cells depending on the number of their connections and how the edges transmit the deformation.

This behavior is very valuable since it allows the structure to naturally nestle to complex shapes, in contrast to traditional flexible materials, like cardboard, fabrics, or sheets of metal.

In general, the deformation behavior of such materials can be controlled by incorporating meso-structures with the desired mechanical properties [Martínez et al. 2019] that may also form elaborate aesthetically pleasing patterns, which can be used to approximate 3D surfaces well.

However, using such complex patterns for inverse shape design leads to two problems: first, their distribution on the surface is a non-trivial geometric task. Second, there is the problem of performance of their simulation.

The structure of a pattern can be very complex and of high geometric resolution, hence its simulation is of significant computational cost. To speed up the optimization process, simplifications need to be made.

In this work we address this problem by simplifying the structure of the pattern by encoding its mechanical properties into the material parameters used in the physical simulation and further performing a homogenization of the meta-material on the coarse level.

Recently, Leimer and Musiański [2020] proposed a structural simplification for such meso-structures to reduce the computational burden by keeping the input-output behaviour. In this paper, we extend this method and propose the following:

- (1) We introduce a pattern generator that is capable of creating flexible hexagonal or rectangular patterns whose flexibility can be locally controlled.
- (2) We propose an optimization scheme for encoding the deformation behavior of a structurally complex pattern into the material parameters of a simple pattern, thus greatly reducing the computational cost of physical simulation.
- (3) We apply our proposed method to the task of shape design by formulating an optimization problem that aims to find the ideal boundary constraints for a flexible pattern such that the pattern deforms to approximate a given target shape.

2 RELATED WORK

The popularity of modern additive manufacturing techniques has led to many advancements in the field of computational design of meta-materials. Increased attention has been given to the possibility of building 3D objects out of volumetric structures composed of regular [Panetta et al. 2015] as well as stochastically sampled [Martínez et al. 2017] grids. Another branch are flat flexible material sheets [Malomo et al. 2018] which can be used to form 3D surfaces. Their advantage is additionally that they can be easily adapted to various shapes and easily produced, transported and assembled on site.

The materials we aim at can be classified as cellular structures, i.e., they consist of more or less regular cellular elements. The research of such structures has been approached across various disciplines due to their very interesting properties. They have been shown to be mechanically extremely efficient since they are very robust and can absorb impacts from large impulse forces on the

one hand, but are of extremely low-density and thus lightweight and flexible on the other [Wadley et al. 2003].

Especially the case of so-called honey-comb structures, which primarily consist of hexagonal elements, has been studied extensively in the fields of mechanical engineering and material sciences, where computational models for their mechanics, i.e., how the structure responds to forces, have been introduced [Gibson et al. 1982; Masters and Evans 1996]. Also the influence of the wall thickness variations on the elastic properties [Li et al. 2005], and the effects of hierarchy [Taylor et al. 2011] have been studied. Moreover, in the fields of geometry and architectural design, cellular and honey-comb like structures have been studied [Jiang et al. 2014; Pottmann et al. 2015] since they are very well suitable for the design of aesthetically and visually pleasing and mechanically stable shapes.

Computational Design. Computational design problems aim at the automatic computation of structural or mechanical designs that suit some desired goals. They have been studied in computational industrial design as form-finding problems, as well as in statics and mechanical engineering as structural optimization problems [Haftka and Gürdal 1992]. In the field of computer graphics and computational geometry such problems often arise in combination with the design of optimal surface meshes that need to fulfill certain goals, mainly in the field of architectural and industrial design [Deng et al. 2015; Panozzo et al. 2013; Pottmann et al. 2007, 2008; Tang et al. 2014; Vouga et al. 2012]. Due to the advances in the digital fabrication field, such problems increasingly arise in various personal fabrication design tasks [Dumas et al. 2015; Garg et al. 2014; Skouras et al. 2014]. Of particular relevance to our work is the design of structures made out of rod-like elements [Malomo et al. 2018; Panetta et al. 2019; Pérez et al. 2015; Pillwein et al. 2020; Vekhter et al. 2019; Zehnder et al. 2016], which is made possible through efficient methods of simulating the deformation behavior of such elements [Bergou et al. 2010, 2008].

Geometry Processing. Between geometry acquisition and some concrete production lies the discipline of digital geometry processing, a relatively new field of computer science that is concerned with mathematical models and algorithms for analyzing and manipulating geometric data [Botsch et al. 2010]. The mapping of polygonal meshes into the plane, or planar deformations and surface parameterizations are two prominent examples [Lipman 2012]. Another related problems are interactive methods for surface mesh deformations [Lipman et al. 2005; Sorkine 2006; Sorkine and Alexa 2007].

Material Simulation. Physical simulation of materials has a long tradition in computer graphics [Terzopoulos et al. 1987], however, they have been usually studied for the sake of virtual materials in animations or surgery simulations [Nealen et al. 2006]. More recently, due to the emergence of the 3d-printing paradigm, computer graphics researchers turned towards real material simulation methods. For instance, Bickel et al. developed in a series of articles a computational system for data-driven design of non-linear elastic materials, e.g., soft tissues [Bickel et al. 2010, 2009]. Their approach provides also goal-based material design which partially inspired our approach.

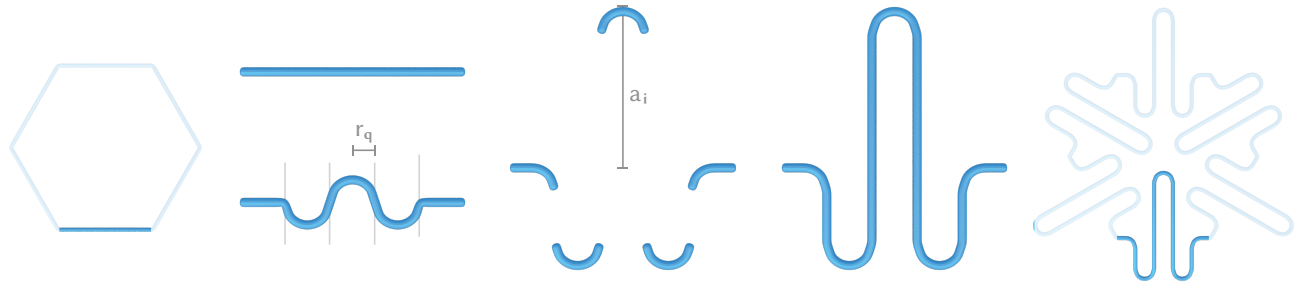


Figure 2: Transforming a hexagon edge into a zig-zag spring. The segments of the edge are replaced by semicircles with radius r_q , which are then offset in y -direction by amplitude a_i .

Other scientific and engineering fields also research the mechanics of cellular meta-materials [Ion et al. 2016; Schaedler and Carter 2016; Zheng et al. 2014] due to their strong structural properties and light-weightness [Zheng et al. 2014]. Unstructured cell distribution, like foams [Ashby 2006], and nano-materials [Meza et al. 2014] belong to this category in the broadest sense as well. An additional advantage of such structures is that they allow to program specific properties, like negative Poisson ratio [Clausen et al. 2015], or adaptable mechanical structures [Jenett et al. 2017].

3 META-MATERIAL DESIGN OVERVIEW

We focus on flat sheets of elastic meta-materials which can be fabricated in planar configurations. Such flat sheets can be bent into spacial surfaces of desired shape if programmed accordingly. They obtain their shape and properties also due to the stress which is constantly stored in the structure if spanned in a precomputed configuration.

The first step in the design of such materials is to choose which type of pattern and meso-structure to use. For the pattern, we decide on a regular tiling of hexagons which allow for regular tessellation of the Euclidean plane. For the meso-structure, we use a type of spring which we will refer to as *zig-zag springs*. To create this meso-structure, we transform each hexagon edge by introducing a natural rest curvature in the underlying 2D plane so that instead of a straight line we obtain a winding curve (see Figure 2 for an example). The number of windings and their amplitude are the free parameters of this meso-structure. The process of creating these patterns is explained in further detail in Section 4.

We use a physical simulation based on the Discrete Elastic Rod (DER) formulation [Bergou et al. 2010, 2008] to approximate the deformation behavior of the pattern. For this purpose, appropriate material parameters are necessary to achieve a realistic behavior. Usually, these values are set based on empirical experiments with the corresponding real world materials. However, simulating the deformation behavior of such complex patterns comes with a high computational cost. To alleviate this problem, we want to look at the pattern at a lower level of detail by simplifying each meso-structure to a simple straight edge made of a meta-material with different material parameters instead.

As an example, pulling at the ends of a zig-zag spring causes in-plane bending in certain regions of the meso-structure. However, when looking at the corresponding edge in the simplified pattern,

which is the straight line connecting the ends of the zig-zag edge, this deformation corresponds to stretching of the edge instead. Thus, to properly imitate this deformation behavior in the simplified pattern, we need to treat the meta-material of the simplified pattern as extensible even though the real-world material of the pattern is not. This is done by choosing appropriate meta-material parameter values. The process of how we optimize these parameters such that the deformation behavior of the simplified pattern matches that of the original pattern is explained in Section 5.

Furthermore, we would like to use the simplified pattern for the purpose of shape design. Since the deformation behavior of flexible patterns is very complex, it can be difficult to figure out how a pattern must be deformed to approximate a desired target shape. In Section 6 we propose an optimization scheme to find the optimal positions and directions of a set of boundary constraints such that the pattern deforms into the desired shape.

We demonstrate the results of our proposed framework in Section 7 and discuss potential future work in Section 8. Finally, we conclude this paper in Section 9.

4 MESO-PATTERN GENERATION

In this section we explain how we generate the complex patterns that we use as examples throughout our work. Our pattern generator is capable of creating regular tilings of either quads or hexagons containing zig-zag springs as edges that control the deformation behavior of the pattern. By extension, it is also possible to create triangular tilings by triangulation, but the lack of space within the triangles makes them ill-suited for containing zig-zag springs.

For the remainder of this work, we will mostly focus on hexagonal tilings for a number of reasons. First, hexagons are one of only three polygon types that allow for regular tilings, the others being triangles and rectangles [Jiang et al. 2015]. Second, the even number of edges allows for a consistent orientation of the zig-zag springs—when traversing the edges of a hexagon, the middle peak of the zig-zag springs always alternates between pointing inward and outward on consecutive edges. Finally, from the perspective of meta-materials, a hexagonal pattern leads to isotropic material behavior [Schumacher et al. 2018]. While rectangles also have the second property, their meta-material behavior only shows a tetragonal symmetry.

Our pattern generation process consists of two main steps, followed by an optional post-processing step. In the first step, we

generate a regular tiling of polygons that serves as the coarse structure of the pattern. Then we transform the edges of the tiling to create the final pattern. Finally, we prepare the pattern for the simulation stage by removing potential causes for error and adjusting the resolution of the pattern.

The input parameters for the first step include the coordinates of the origin c_0 , which is the center of the bottom left element of the tiling, the number of elements in x- and y-direction, as well as the circumradius r of the elements. The output consists of vertices V , faces F and edges E , as well as a vector s containing a sign for each edge that determine the winding direction of the transformed edge.

For creating a hexagonal tiling, we first compute the center position of each hexagon based on the origin and circumradius. The hexagon centers c_i of the first row are given by

$$c_i = c_0 + \sum_{j=0}^{i-1} r \begin{bmatrix} 1 + \sin(\pi/3) \\ (-1)^j \cos(\pi/3) \end{bmatrix}.$$

The hexagon centers of any other row can be computed by simply offsetting the centers of the previous row by $d = 2r \sin(\pi/3)$ in y-direction, which is the diameter of the hexagon incircle.

Then the position of each corner vertex is computed by offsetting each hexagon center by $(\cos(\frac{i\pi}{3}), \sin(\frac{i\pi}{3}))$ with $i = 0, \dots, 5$. We create a face matrix F with one row per hexagon, each containing the indices of the corresponding hexagon vertices. Since this process creates six vertices per hexagon, we afterwards weld the pattern by removing duplicate vertices and updating their indices in the face matrix. To create the list of signs s , we simply traverse each hexagon edge-by-edge while alternating between 1 and -1 , only appending the value to the list if the current edge has not been visited before.

In the second step, we transform each hexagon edge into a zig-zag spring. This operation takes a vector of amplitudes a as input - the length n of the vector determines the number of peaks, while the values a_i with $0 \leq a_i \leq 1$ determine the height of each peak. The computations in this step are performed in the local coordinate system of each edge, with the edge being parallel to the x-axis with start point $(0, 0)$ and end point $(1, 0)$ and the hexagon center being located at $(0.5, 1)$. Therefore the amplitudes a_i are given relative to the radius of the hexagon incircle.

We partition each edge into $n + 2$ segments. Every segment excluding the first and last segment, which are treated separately, is replaced by a semicircle. The radius of the semicircle is given by $r_q = 1/(2(n + 2))$. We use the top or bottom half of a circle depending on the sign of the peak $\hat{s}_i = s_e(-1)^i$, where the sign s_e of edge e determines the overall direction of the zig-zag spring, while $(-1)^i$ causes the direction of consecutive peaks to alternate. The semicircle centers are then offset in y-direction by $\hat{s}_i(a_i - r_q)$. In other words, the amplitude a_i of the i -th peak determines how far each semicircle is moved from the original edge, with the positive or negative direction depending on the sign of the peak. In the special case that $a_i < r_q$, we replace the semicircle with a semi-ellipse of width r_q and height a_i .

For the first segment of the edge, we leave the first half as it is and replace the second half by a quarter circle such that it can connect to the next segment without self-intersections. The last

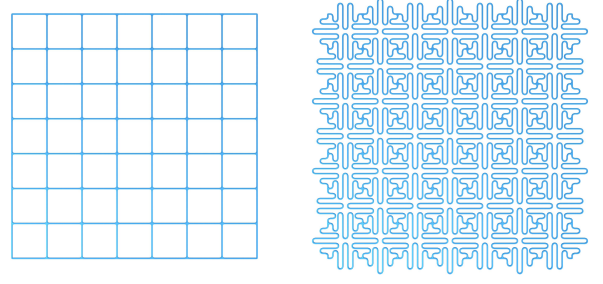


Figure 3: An example of a pattern based on a rectangular tiling. While the orientation of zig-zag springs in patterns consisting of hexagons is the same for each cell, they are inverted for each pair of adjacent rectangles.

segment is treated similarly, but mirrored horizontally. Please refer to Figure 2 for a visual depiction.

Finally, we perform one additional post-processing step as preparation for simulating the deformation behavior of the pattern. We first remove any zero-length edges in the pattern—these can occur in cases where $a_i < r_q$ since the start and end point of consecutive peaks become identical. Then we subdivide any edges that are longer than a user-provided maximum to ensure that the resolution of the pattern is sufficiently high.

The generation of a rectangular pattern is handled in a similar manner. The main difference is how the list of signs s is created. Just like with the hexagonal tiling, we traverse the pattern edge-by-edge, alternating between positive and negative signs. For the rectangular tiling however, we additionally make sure that the signs of adjacent rectangles are inverted. An example can be seen in Figure 3.

5 MESO-PATTERN SIMPLIFICATION

As mentioned previously, simulating the deformation behavior of such complex meso-patterns has a high computational cost. Our goal is to reduce this cost by simplifying the pattern, encoding the structural properties of the complex pattern into the material parameters of the simplified pattern instead. In this section we explain this process.

Consider two patterns, a complex pattern T and a simple pattern S , that are generated from the same tiling. T is generated by replacing the edges of the tiling by zig-zag springs (see Section 4), while the simple pattern S is created by subdividing the edges. The deformation behavior of these patterns can then be simulated, which is explained in Section 5.1. Within the simulation, we treat each edge of the original tiling as a flexible rod which is connected to other rods at the vertices of the original tiling. Therefore, both the complex pattern T and the simple pattern S have the same number of rods and the same number of connections where the ends of these rods meet. We denote the position of these connections as V_T and V_S , and the material directions at these connections as N_T and N_S for the complex pattern T and simple pattern S respectively. This direct correspondence between the connections of the complex and simple pattern makes it easier to compare the deformation behavior of the two patterns by directly comparing the positions

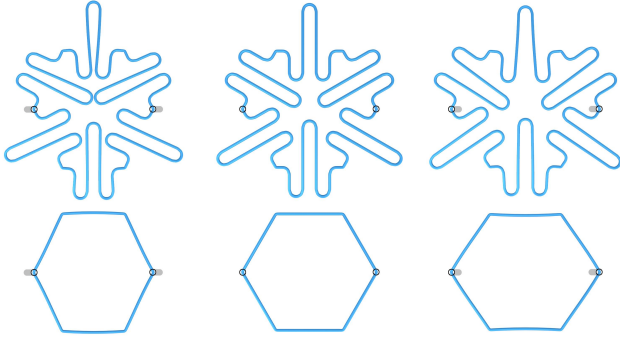


Figure 4: Deformation behavior when the anchor constraints (circles) are moved toward or away from the center. The corner vertices of the simple hexagons (bottom) match their corresponding vertices of the complex hexagons (top).

V_T and material directions N_T of the deformed complex pattern with V_S and N_S of the deformed simple pattern.

Since the structure of the simple pattern is very different from the complex pattern, the deformation behavior will also be different. For the simple pattern to imitate the deformation behavior of the complex pattern, it is necessary to find appropriate material-parameters k_S that encode the structural properties of the zig-zag edges of the complex pattern into the meta-material properties of the straight edges of the simple pattern. We do this by formulating an optimization problem which is explained in Section 5.2.

5.1 Simulation

Our physical simulation is based on the Discrete Elastic Rods (DER) formulation [Bergou et al. 2010, 2008], treating each hexagon edge as a rod. Additionally, the corner vertices of the hexagons where multiple rods come together are treated as rigid-body connections [Pérez et al. 2015] whose orientation is defined by additional degrees of freedom [Zehnder et al. 2016]. This formulation allows the computation of the elastic stretching, bending and twisting energies of each rod under a set of constraints, based on the geometry of the pattern, and to find the equilibrium state of the structure by minimizing the elastic energy. Building upon the framework of Vekhter et al. [2019], we formulate an optimization problem to find this equilibrium state of the pattern by minimizing the energy functional

$$E_{rod} = E_r + E_a,$$

where E_r is the internal energy of the rods consisting of stretching, bending and twisting energies and E_a denotes the energy of the anchor constraints. For a detailed explanation of the internal energy, we refer the reader to the work of Bergou et al. [2010]. A single anchor constraint is defined by a vector of size 9. The first 3 entries consist of a rod index, segment index i and barycentric coordinate β that specify the point $p = (1-\beta)p_i + \beta p_{i+1}$ on the corresponding rod. The other entries define the target position p_a and material vector direction m_a , leading to the definition of the anchor constraint energy

$$E_a = \|p - p_a\|^2 + \phi(m, m_a)^2, \quad (1)$$

with the function

$$\phi(m, m_a) = 2 \operatorname{atan2} \left((m \times m_a)^T (m \times m_a), \|m\| \|m_a\| + m^T m_a \right)$$

returning the angle between the material vector m of segment i and the target direction m_a .

5.2 Material Parameter Optimization

Aside from the geometry of the pattern, the deformation behavior is determined by the respective material parameters k_T and k_S . This includes the stiffness for stretching, bending and twisting of the rods, as well as the thickness and width of the rod cross section. The material parameters k_T for the complex pattern are set based on the real world material used for fabricating the pattern. Our goal is then to find the optimal material parameters k_S for the simple pattern, such that the deformation behavior of the simple pattern matches that of the complex one.

For this optimization process, we first simulate the deformation of both patterns under a set of anchor constraints A . We can then define the difference between the two deformed patterns as the energy

$$E_{\text{simpl}}(A, k_S) = \|V_T(A) - V_S(A, k_S)\|^2 + \|1 - \langle N_T(A), N_S(A, k_S) \rangle\|^2,$$

which measures the distance between the positions of the rod connections V_T and V_S , as well as the difference in material directions N_T and N_S .

Our goal is to find material parameters k_S that minimize this energy. However, a single deformed target shape might not contain enough information about the deformation behavior of the pattern. For example, an in-plane deformation of the pattern as demonstrated in Figure 4 does not yield any information about the out-of-plane bending and twisting behavior of the rods. To make sure the space of possible deformations is sufficiently covered, we therefore try to minimize the objective function over multiple sets of anchor constraints A_i . The optimization problem we want to solve is therefore given as

$$\min_{k_S} \sum_i E_{\text{simpl}}(A_i, k_S). \quad (2)$$

For the optimization process, we make use of the Sequential Quadratic Programming (SQP) algorithm [Nocedal and Wright 2006] to minimize the objective function. Since we only want to optimize a small set of parameters, we compute the gradient of the objective function numerically.

6 SHAPE DESIGN AND OPTIMIZATION

Once we have found the appropriate material parameter values for the simplified pattern, we can use them for applications like shape design. As an example, we will consider a pattern P that can be deformed by constraining the position and normal direction at specified points on the pattern using a set of anchors A .

As explained in Section 5.1, anchors A are given as a matrix with one row per anchor and 9 columns. For each anchor, the first 3 columns contain the rod index, segment index and barycentric coordinate β that specify the point p on the pattern that is constrained. These values remain fixed during the optimization process. The remaining entries are the target position and material direction.

Our goal is now to find the optimal anchor positions and material directions such that pattern P in the deformed state matches the deformed target pattern Q .

6.1 Optimization problem

Let p and q be the respective vertex positions and m and n be the respective material frame vectors for patterns P and Q . Similar to the pattern simplification problem, we formulate the optimization problem as

$$\min_A E_{\text{shape}}(A), \quad (3)$$

where

$$E_{\text{shape}}(A) = \|q - p(A)\|^2 + \|1 - \langle n, m(A) \rangle\|^2. \quad (4)$$

To solve this optimization problem, we first simulate the deformation of the pattern P using an initial guess for the anchors A_0 . With this deformed pattern P_0 as an initial state, we again use the SQP-algorithm to solve the optimization problem. Within each iteration i , the deformation of the pattern is simulated and the objective function and its gradient are evaluated to compute the anchors A_{i+1} for the next iteration. Furthermore, since we need to optimize 6 variables per anchor, we compute the analytical gradient of the objective function, which is explained in the next section.

6.2 Gradient

Let x be the vector of all state variables of the DER simulation (in our case the vertex positions p and material frame vectors m) and let u be the vector of design variables (in our case the target positions and material directions of anchors A). Then the analytical gradient of the objective function is given by

$$\frac{\partial E_{\text{shape}}}{\partial u} = \frac{\partial E_{\text{shape}}}{\partial x} \frac{\partial x}{\partial u} \quad (5)$$

The derivative $\partial x / \partial u$ is unknown. However, we can compute this derivative by means of sensitivity analysis in a similar manner to [Malomo et al. 2018] and [Panetta et al. 2019]. We want any change of the design variables to preserve the equilibrium state of the deformed pattern, meaning that the derivative of the forces f acting on the pattern should vanish. Thus we have

$$\delta f = \frac{\partial^2 E_{\text{rod}}}{\partial x \partial x} \frac{\partial x}{\partial u} \delta u + \frac{\partial^2 E_{\text{rod}}}{\partial x \partial u} \delta u = 0,$$

with E_{rod} being the elastic energy of the pattern in the deformed state. We can now solve for $\partial x / \partial u$ directly with

$$\frac{\partial x}{\partial u} = - \left(\frac{\partial^2 E_{\text{rod}}}{\partial x \partial x} \right)^{-1} \frac{\partial^2 E_{\text{rod}}}{\partial x \partial u}, \quad (6)$$

or use the more efficient adjoint method by inserting Equation 6 into Equation 5 to get

$$\frac{\partial E_{\text{shape}}}{\partial u} = - \frac{\partial E_{\text{shape}}}{\partial x} \left(\frac{\partial^2 E_{\text{rod}}}{\partial x \partial x} \right)^{-1} \frac{\partial^2 E_{\text{rod}}}{\partial x \partial u} = \lambda^T \frac{\partial^2 E_{\text{rod}}}{\partial x \partial u},$$

and solving for λ :

$$\lambda = - \left(\left(\frac{\partial^2 E_{\text{rod}}}{\partial x \partial x} \right)^{-1} \right)^T \left(\frac{\partial E_{\text{shape}}}{\partial x} \right)^T$$

Based on the DER formulation, we compute the bending and twisting energies at each vertex, the stretching energies at each

edge, as well as the position- and direction constraint energies for each anchor. For ease of implementation, we only compute the square root of these terms and store them in the vector r , such that the total elastic energy of the system is then given by $E_{\text{rod}} = r^T r$. The first and second derivatives of the elastic energies are therefore given by

$$\frac{\partial E_{\text{rod}}}{\partial x} = 2 J_x^T r,$$

$$\frac{\partial^2 E_{\text{rod}}}{\partial x \partial x} = 2 \left(J_x^T J_x + r^T H_{xx} \right),$$

$$\frac{\partial^2 E_{\text{rod}}}{\partial x \partial u} = 2 \left(J_x^T J_u + r^T H_{xu} \right),$$

with J being the Jacobian matrix

$$J_x = \frac{\partial r}{\partial x},$$

and H being the 3-dimensional Hessian tensor

$$H_{xx} = \frac{\partial^2 r}{\partial x \partial x}.$$

For detailed explanation of the derivatives of the stretching, bending and twisting energies we refer the reader to the work of Panetta et al. [2019], particularly the supplementary material. For the derivatives of the anchor constraint terms, we refer the interested reader to Appendix A.

7 RESULTS

In this section we perform a number of experiments to evaluate our proposed framework. We first demonstrate our pattern simplification method in Section 7.1, followed by our shape optimization in Section 7.2.

7.1 Simplification results

The top of Figure 4 shows an example of how a single hexagon cell with meso-structures deforms when moving the two anchor points marked by circles along the x-axis. For the simplified hexagon cell (bottom), this in-plane bending deformation corresponds to both stretching and in-plane bending of the edges. By finding appropriate material stiffness parameters, the coordinates of the corner vertices become identical for both the complex and simplified cells.

Figure 5 shows larger patterns made of 7×6 hexagon cells simulated using our approach. The complex patterns on the left contain 12643 vertices and 12684 edge segments, while the simplified patterns on the right only contain 563 vertices and 604 edge segments, significantly reducing the computational cost of the simulation while yielding a good approximation of the resulting deformed patterns.

As an experiment, we use the proposed method to find the optimal parameters for the patterns shown in Figure 8. In all examples we use a structure of 7×6 hexagon cells with a circumradius of 7mm and origin coordinates $c_0 = (0, 0)$. The cross-section of the complex pattern is 0.6mm wide and 3mm thick. For this experiment, we set the stiffness parameters with regards to stretching, bending and twisting to 10^{10} , 10^6 and 10^6 respectively. Together with the width and thickness of the cross-section, they form the material parameters k_T . For the simple pattern, we subdivide each hexagon edge into 4 segments. The material parameters k_S which we want

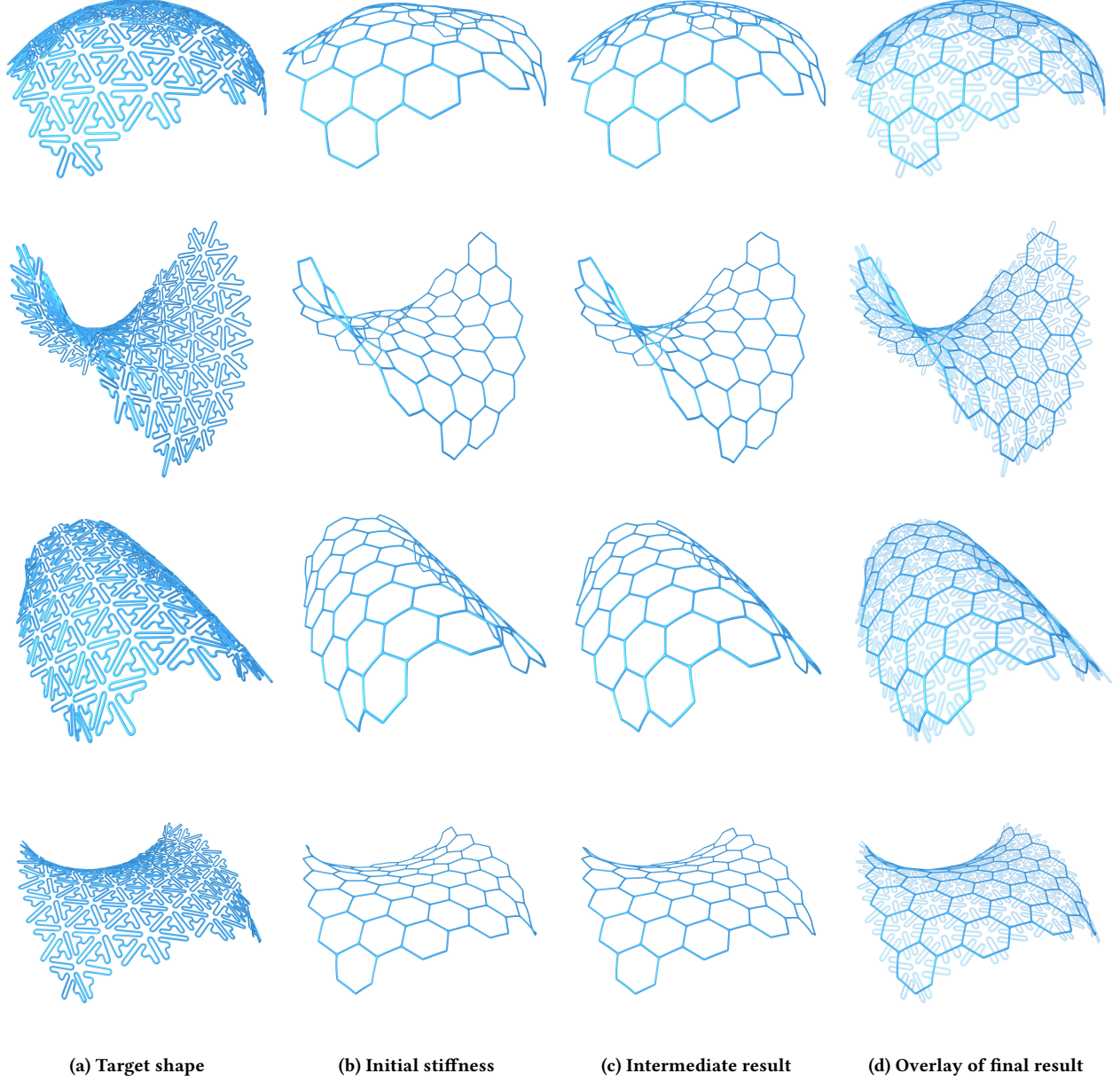


Figure 5: Results of the material parameter optimization. (a) Deformed pattern that serves as the target shape. (b) Simple pattern with initial material parameter values. (c) Simple pattern after a few iterations of optimization. (d) Overlay of optimized simple pattern with target shape.

to optimize are initialized as 10^6 for the stretching, bending and twisting stiffness and $1mm$ for both the thickness and width of the cross-section. We define 4 sets of anchors to deform the patterns into the shapes shown on the left of Figure 8, which we will refer to as Dome, Saddle, Tunnel and Manta from top to bottom. The structure of the pattern and the vertices constrained by the anchors are the same for each target shape, only the prescribed positions and

material directions at these vertices differ for each set of anchors. Please refer to Figure 1 for a comparison to the fabricated examples. We first simulate the complex pattern for each set of anchors to obtain the target shapes T_j with $j = 1, \dots, 4$.

To evaluate the objective function, the simple pattern is simulated once for each set of anchors to obtain S_j for the current iteration of the optimization. Using all four shapes as targets, the

Table 1: Evaluation of the optimized stiffness parameters. Each column shows which target shape was used in the optimization. The values show the average distance between corresponding corner vertices of the complex and simple pattern in millimeters (the size of the full pattern is 87mm by 83mm).

Evaluated Shape	Target Shape				
	All	Dome	Saddle	Tunnel	Manta
Dome	0.0940	0.0823	2.2855	0.2273	0.1523
Saddle	0.1271	0.1696	0.2737	0.1996	0.1787
Tunnel	0.1525	0.1826	3.0581	0.1234	0.2036
Manta	0.2284	0.3901	1.5823	0.2401	0.2062

optimization process takes 291 seconds on average and the resulting material parameters k_S are $0.034 \cdot 10^6$, $0.79 \cdot 10^6$ and $1.48 \cdot 10^6$ for the stretching, bending and twisting stiffness respectively, as well as cross-sectional thickness 1.54mm and width 0.61mm. Table 1 shows the average distance between corresponding corner vertices of the complex and simple pattern in millimeters (the size of the full pattern is 87mm by 83mm). As an additional experiment, we perform the optimization using only a single target shape each. The computation times range from 66 seconds for the Dome shape to 107 seconds for the Manta shape. As can be seen in Table 1, the quality of the optimization result greatly depends on the used target shape. Using only the Dome or Saddle shapes as targets results in significantly worse results overall, while the Tunnel or Manta shape yield a better approximation. This suggests that the deformations of the Tunnel and Manta shapes contain more information about the deformation behavior of the pattern than the Dome or Saddle shapes.

To compare the computational cost of the original and simplified patterns, we simulate the deformation of both patterns for each of the four target shapes and record the time until an equilibrium state is reached. For the original pattern, simulation takes 16.04, 21.81, 21.35 and 30.68 seconds for the Dome, Saddle, Tunnel and Manta shapes respectively. For the simplified patterns, we obtain simulation times of 0.85, 0.87, 0.61 and 1.07 seconds respectively, which corresponds to a reduction of computation time ranging from 94.70 to 97.13 percent.

7.2 Shape optimization results

To evaluate our shape optimization method, we follow the example described in Section 6. Our input is a flat pattern and four anchor constraints whose initial values correspond to the location and material direction of the four corners of the pattern. The material parameters k_S of the pattern are set to the optimized values we obtained in the pattern simplification step described in Section 7.1. Our goal is to deform the pattern into the target shape by finding the optimal values for the anchor constraints. As targets we use the four shapes shown on the right of Figure 5 that are the result of our pattern simplification process. Once again we use the SQP algorithm to solve the optimization problem. Figure 6 shows the intermediate and final results for the shape optimization, while Table 2 shows the quantitative evaluation in terms of objective function value (see Equation 4), average distance between vertices

Table 2: Evaluation of the shape optimization experiment. The columns show the objective function value (see Equation 4), average distance between vertices in millimeters, number of optimization iterations and computation time for each of the four target shapes.

Shape	E_{shape}	Avg. Distance	Iterations	Time
Dome	0.0079	0.0724mm	93	547s
Saddle	0.0489	0.1678mm	60	599s
Tunnel	0.0305	0.1317mm	102	1070s
Manta	0.3185	0.4385mm	54	445s

in millimeters, number of optimization iterations and computation time. Finally, Figure 7 shows a logarithmic plot of how the shape energy term E_{shape} changes during the course of the optimization.

To compare the computational cost of shape optimization using a complex pattern against using a simplified pattern, we perform an additional test with a smaller pattern size consisting of 3x3 hexagon cells. For the target deformation we use a Dome shape with anchor constraint parameters scaled to fit the smaller pattern size. The optimization process using the simplified pattern takes 64.1 seconds, while using the complex pattern results in a time of 6115.2 seconds. However, it must be noted that our implementation of the Hessian computation is not well optimized for large grids with high complexity and can likely be improved for better scaling.

7.3 Implementation

All our algorithms for pattern generation, pattern simplification and shape optimization are implemented in MATLAB, using the SQP algorithm to solve the optimization problems defined in Equations 2 and 3. The DER simulation is implemented in C++, building upon the framework of Vekhter et al. [2019]. For fabrication, we additionally make use of the 3d-modeling software Rhinoceros with parametric modeling plugin Grasshopper to create a 3d-printable mesh. The pattern is then fabricated using an Ultimaker 3 3d-printer.

8 FUTURE WORK

In the future, we would like extend our method to compute the gradient of the objective function analytically by means of sensitivity analysis. The gain in speed would allow us to consider per-edge stiffness parameters instead of global parameters to account for local variations in deformation behavior (see Figure 8 for an example).

We would furthermore like to examine the relationship between the free parameters of our meso-structure and the stiffness parameters of the simplified grid. Creating a mapping between these two sets of parameters would make it possible to reverse the grid simplification process, allowing us to perform shape optimization with the simplified pattern using the local stiffness parameters as design variables, then replacing the hexagon edges with the appropriate zig-zag springs that yield the desired deformation behavior.

Finally, we have only considered the use of regular tilings for the generation of our patterns so far. However, it may not be possible to approximate very complex shapes using such tilings. In the future, it would be interesting to consider the use of non-regular tilings and how such tilings can be generated for the best possible approximation of the target shape.

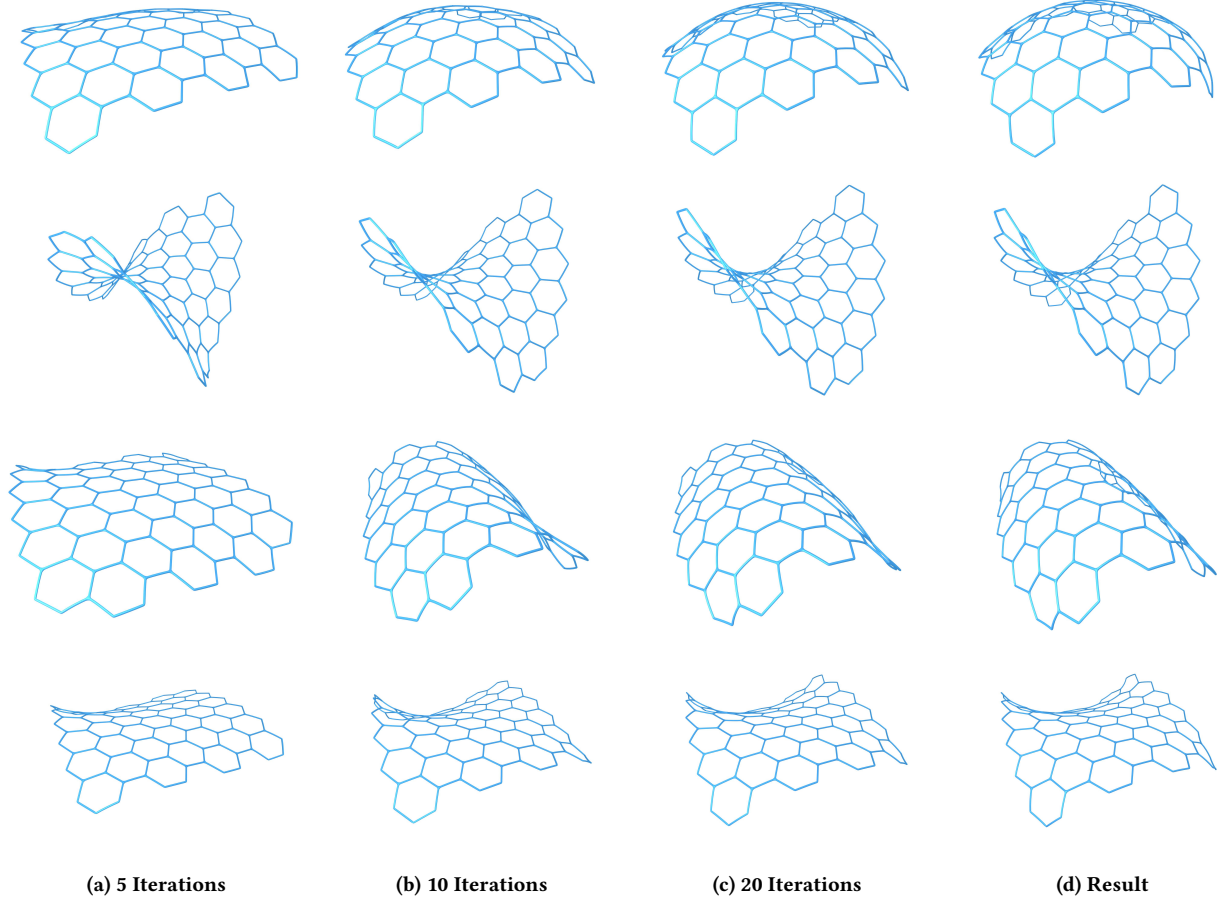


Figure 6: Shape optimization results. Starting with a flat pattern, the position and material direction of the anchor constraints at the four corners of the pattern are optimized to deform the pattern into the target shape.

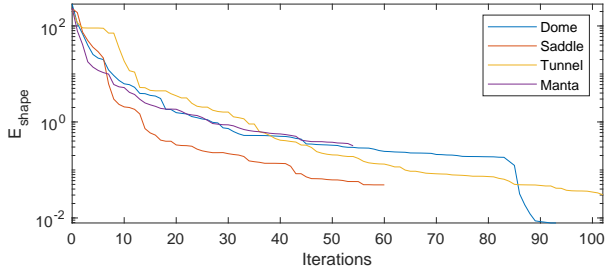


Figure 7: Plot of the objective value E_{shape} during shape optimization. The x-axis shows the number of iterations, while the y-axis shows the objective value on a logarithmic scale.

9 CONCLUSIONS

We presented a framework for the generation and optimization of reduced order flexible patterns. Our pattern generator is capable of creating complex patterns based on hexagonal or rectangular

tilings whose deformation behavior can then be simulated. Since the simulation of such complex patterns has a high computational cost, we simplify the pattern by encoding the complex deformation behavior of the structure into the meta-material parameters of a more simple pattern. The simple pattern can then be used for shape design, which we demonstrated by finding the optimal boundary constraints that deform the pattern into the desired target shape.

ACKNOWLEDGMENTS

This research was funded by the Vienna Science and Technology Fund (WWTF ICT15-082).

REFERENCES

- Michael F Ashby. 2006. The properties of foams and lattices. *Philosophical Transactions of the Royal Society A: Mathematical, Physical and Engineering Sciences* 364, 1838 (2006), 15–30.
- Miklós Bergou, Basile Audoly, Etienne Vouga, Max Wardetzky, and Eitan Grinspun. 2010. Discrete viscous threads. *ACM Transactions on Graphics (TOG)* 29, 4 (2010), 1–10.
- Miklós Bergou, Max Wardetzky, Stephen Robinson, Basile Audoly, and Eitan Grinspun. 2008. Discrete elastic rods. In *ACM SIGGRAPH 2008 papers*. 1–12.

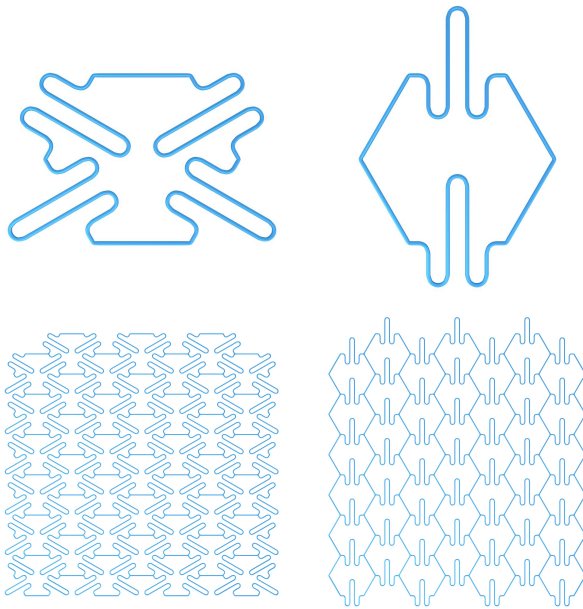


Figure 8: Different cell types created by changing the input parameters to our pattern generator.

- Bernd Bickel, Moritz Bächer, Miguel A. Otaduy, Hyunho Richard Lee, Hanspeter Pfister, Markus Gross, and Wojciech Matusik. 2010. Design and fabrication of materials with desired deformation behavior. *ACM Transactions on Graphics* 29, 4 (jul 2010), 1. <https://doi.org/10.1145/1778765.1778800>
- Bernd Bickel, Moritz Bächer, Miguel A. Otaduy, Wojciech Matusik, Hanspeter Pfister, and Markus Gross. 2009. Capture and modeling of non-linear heterogeneous soft tissue. *ACM Transactions on Graphics* 28, 3 (jul 2009), 1. <https://doi.org/10.1145/1531326.1531395>
- M Botsch, L Kobbelt, M Pauly, P Alliez, and B Levy. 2010. *Polygon Mesh Processing*. Taylor & Francis. <http://books.google.at/books?id=8zX-2VRqBAkC>
- Anders Clausen, Fengwen Wang, Jakob S Jensen, Ole Sigmund, and Jennifer A Lewis. 2015. Topology optimized architectures with programmable Poisson's ratio over large deformations. *Adv. Mater* 27, 37 (2015), 5523–5527.
- Bailin Deng, Sofien Bouaziz, Mario Deuss, Alexandre Kaspar, Yuliy Schwartzburg, and Mark Pauly. 2015. Interactive design exploration for constrained meshes. *Computer-Aided Design* 61 (apr 2015), 13–23. <https://doi.org/10.1016/j.cad.2014.01.004>
- Jérémy Dumas, An Lu, Sylvain Lefebvre, Jun Wu, and Christian Dick. 2015. By-example synthesis of structurally sound patterns. *ACM Transactions on Graphics (TOG)* 34, 4 (2015), 1–12.
- Akash Garg, Andrew O. Sageman-Furnas, Bailin Deng, Yonghao Yue, Eitan Grinspun, Mark Pauly, and Max Wardetzky. 2014. Wire mesh design. *ACM Transactions on Graphics* 33, 4 (jul 2014), 1–12. <https://doi.org/10.1145/2601097.2601106>
- L J Gibson, M F Ashby, G S Schajer, and C I Robertson. 1982. The Mechanics of Two-Dimensional Cellular Materials. *Proceedings of the Royal Society A: Mathematical, Physical and Engineering Sciences* 382, 1782 (jul 1982), 25–42. <https://doi.org/10.1098/rspa.1982.0087>
- Raphael T. Haftka and Zafer Gürdal. 1992. *Elements of Structural Optimization* (3rd rev. a ed.). Springer. http://books.google.at/books/about/Elements_of_Structural_Optimization.html?id=Czglpexeh7UC&pgis=1
- Alexandra Ion, Johannes Frohnhofer, Ludwig Wall, Robert Kovacs, Mirela Alistar, Jack Lindsay, Pedro Lopes, Hsiang-Ting Chen, and Patrick Baudisch. 2016. Metamaterial mechanisms. In *Proceedings of the 29th Annual Symposium on User Interface Software and Technology*. 529–539.
- Benjamin Jenett, Sam Calisch, Daniel Cellucci, Nick Cramer, Neil Gershenfeld, Sean Swee, and Kenneth C Cheung. 2017. Digital morphing wing: active wing shaping concept using composite lattice-based cellular structures. *Soft robotics* 4, 1 (2017), 33–48.
- Caigui Jiang, Chengcheng Tang, Amir Vaxman, Peter Wonka, and Helmut Pottmann. 2015. Polyhedral patterns. *ACM Transactions on Graphics (TOG)* 34, 6 (2015), 1–12.
- Caigui Jiang, Jun Wang, Johannes Wallner, and Helmut Pottmann. 2014. Freeform Honeycomb Structures. *Computer Graphics Forum* 33, 5 (aug 2014), 185–194. <https://doi.org/10.1111/cgf.12444>
- Kurt Leimer and Przemysław Musiański. 2020. Simulation of Flexible Patterns by Structural Simplification. In *ACM SIGGRAPH 2020 Posters on - SIGGRAPH '20*. ACM Press.
- K. Li, X.-L. Gao, and G. Subhash. 2005. Effects of cell shape and cell wall thickness variations on the elastic properties of two-dimensional cellular solids. *International Journal of Solids and Structures* 42, 5-6 (mar 2005), 1777–1795. <https://doi.org/10.1016/j.ijsolstr.2004.08.005>
- Yaron Lipman. 2012. Bounded distortion mapping spaces for triangular meshes. *ACM Transactions on Graphics* 31, 4 (jul 2012), 1–13. <https://doi.org/10.1145/2185520.2185604>
- Yaron Lipman, Olga Sorkine, David Levin, and Daniel Cohen-Or. 2005. Linear rotation-invariant coordinates for meshes. *ACM Transactions on Graphics* 24, 3 (jul 2005), 479. <https://doi.org/10.1145/1073204.1073217>
- Luigi Malomo, Jesús Pérez, Emmanuel Iarussi, Nico Pietroni, Eder Miguel, Paolo Cignoni, and Bernd Bickel. 2018. FlexMaps: computational design of flat flexible shells for shaping 3D objects. *ACM Transactions on Graphics (TOG)* 37, 6 (2018), 1–14.
- Jonàs Martínez, Méline Skouras, Christian Schumacher, Samuel Hornus, Sylvain Lefebvre, and Bernhard Thomaszewski. 2019. Star-shaped metrics for mechanical metamaterial design. *ACM Transactions on Graphics* 38, 4 (jul 2019), 1–13. <https://doi.org/10.1145/3306346.3322989>
- Jonàs Martínez, Haichuan Song, Jérémy Dumas, and Sylvain Lefebvre. 2017. Orthotropic $\langle i \rangle$ -nearest foams for additive manufacturing. *ACM Transactions on Graphics* 36, 4 (jul 2017), 1–12. <https://doi.org/10.1145/3072959.3073638>
- I.G. Masters and K.E. Evans. 1996. Models for the elastic deformation of honeycombs. *Composite Structures* 35, 4 (aug 1996), 403–422. [https://doi.org/10.1016/S0263-8223\(96\)00054-2](https://doi.org/10.1016/S0263-8223(96)00054-2)
- Lucas R Meza, Satyajit Das, and Julia R Greer. 2014. Strong, lightweight, and recoverable three-dimensional ceramic nanolattices. *Science* 345, 6202 (2014), 1322–1326.
- Andrew Nealen, Matthias Müller, Richard Keiser, Eddy Boxerman, and Mark Carlson. 2006. Physically Based Deformable Models in Computer Graphics. *Computer Graphics Forum* 25, 4 (dec 2006), 809–836. <https://doi.org/10.1111/j.1467-8659.2006.01000.x>
- Jorge Nocedal and Stephen Wright. 2006. *Numerical Optimization*. Springer New York. <https://books.google.at/books?id=VbHYoSyelFcC>
- Julian Panetta, MINA Konaković-Luković, Florin Isvoranu, Etienne Bouleau, and Mark Pauly. 2019. X-shells: A new class of deployable beam structures. *ACM Transactions on Graphics (TOG)* 38, 4 (2019), 1–15.
- Julian Panetta, Qingnan Zhou, Luigi Malomo, Nico Pietroni, Paolo Cignoni, and Denis Zorin. 2015. Elastic textures for additive fabrication. *ACM Transactions on Graphics* 34, 4 (jul 2015), 135:1–135:12. <https://doi.org/10.1145/2766937>
- Daniele Panozzo, Philippe Block, and Olga Sorkine-Hornung. 2013. Designing unreinforced masonry models. *ACM Transactions on Graphics* 32, 4 (jul 2013), 1. <https://doi.org/10.1145/2461912.2461958>
- Jesús Pérez, Bernhard Thomaszewski, Stelian Coros, Bernd Bickel, José A Canabal, Robert Sumner, and Miguel A Otaduy. 2015. Design and fabrication of flexible rod meshes. *ACM Transactions on Graphics (TOG)* 34, 4 (2015), 1–12.
- Stefan Pillwein, Kurt Leimer, Michael Birsak, and Przemysław Musiański. 2020. On Elastic Geodesic Grids and Their Planar to Spatial Deployment. *ACM Transactions on Graphics* 39, 4 (jul 2020), 12. <https://doi.org/10.1145/3386569.3392490>
- Helmut Pottmann, Caigui Jiang, Mathias Höbinger, Jun Wang, Philippe Bompas, and Johannes Wallner. 2015. Cell packing structures. *Computer Aided Design* 60 (mar 2015), 70–83. <https://doi.org/10.1016/j.cad.2014.02.009>
- Helmut Pottmann, Yang Liu, Johannes Wallner, Alexander Bobenko, and Wenping Wang. 2007. Geometry of multi-layer freeform structures for architecture. *ACM Transactions on Graphics* 26, 3 (jul 2007), 65. <https://doi.org/10.1145/1276377.1276458>
- Helmut Pottmann, Alexander Schiffner, Pengbo Bo, Heinz Schmiedhofer, Wenping Wang, Niccolò Baldassini, and Johannes Wallner. 2008. Freeform surfaces from single curved panels. *ACM Transactions on Graphics* 27, 3 (aug 2008), 1. <https://doi.org/10.1145/1360612.1360675>
- Tobias A Schaedler and William B Carter. 2016. Architected cellular materials. *Annual Review of Materials Research* 46 (2016), 187–210.
- Christian Schumacher, Steve Marschner, Markus Gross, and Bernhard Thomaszewski. 2018. Mechanical characterization of structured sheet materials. *ACM Transactions on Graphics (TOG)* 37, 4 (2018), 1–15.
- Méline Skouras, Bernhard Thomaszewski, Peter Kaufmann, Akash Garg, Bernd Bickel, Eitan Grinspun, and Markus Gross. 2014. Designing inflatable structures. *ACM Transactions on Graphics* 33, 4 (jul 2014), 1–10. <https://doi.org/10.1145/2601097.2601166>
- Olga Sorkine. 2006. Differential Representations for Mesh Processing. *Computer Graphics Forum* 25, 4 (dec 2006), 789–807. <https://doi.org/10.1111/j.1467-8659.2006.00999.x>
- Olga Sorkine and Marc Alexa. 2007. As-rigid-as-possible surface modeling. In *Proceedings of the fifth Eurographics symposium on Geometry*. Eurographics Association, 109–116. <http://dl.acm.org/citation.cfm?id=1281991.1282006>

- Chengcheng Tang, Xiang Sun, Alexandra Gomes, Johannes Wallner, and Helmut Pottmann. 2014. Form-finding with polyhedral meshes made simple. *ACM Transactions on Graphics* 33, 4 (jul 2014), 1–9. <https://doi.org/10.1145/2601097.2601213>
- C.M. Taylor, C.W. Smith, W. Miller, and K.E. Evans. 2011. The effects of hierarchy on the in-plane elastic properties of honeycombs. *International Journal of Solids and Structures* 48, 9 (may 2011), 1330–1339. <https://doi.org/10.1016/j.ijsolstr.2011.01.017>
- Demetri Terzopoulos, John Platt, Alan Barr, and Kurt Fleischer. 1987. Elastically deformable models. *ACM SIGGRAPH Computer Graphics* 21, 4 (aug 1987), 205–214. <https://doi.org/10.1145/37402.37427>
- Josh Vekhter, Jiacheng Zhuo, Luisa F Gil Fandino, Qixing Huang, and Etienne Vouga. 2019. Weaving geodesic foliations. *ACM Transactions on Graphics (TOG)* 38, 4 (2019), 1–22.
- Etienne Vouga, Mathias Höbinger, Johannes Wallner, and Helmut Pottmann. 2012. Design of self-supporting surfaces. *ACM Transactions on Graphics* 31, 4 (jul 2012), 1–11. <https://doi.org/10.1145/2185520.2185583>
- H.N.G. Wadley, N.A. Fleck, and A.G. Evans. 2003. Fabrication and structural performance of periodic cellular metal sandwich structures. *Composites Science and Technology* 63, 16 (dec 2003), 2331–2343. [https://doi.org/10.1016/S0266-3538\(03\)00266-5](https://doi.org/10.1016/S0266-3538(03)00266-5)
- Jonas Zehnder, Stelian Coros, and Bernhard Thomaszewski. 2016. Designing structurally-sound ornamental curve networks. *ACM Transactions on Graphics (TOG)* 35, 4 (2016), 1–10.
- Youyi Zheng, Daniel Cohen-Or, Melinos Averkiou, and Niloy J Mitra. 2014. Recurring Part Arrangements in Shape Collections. *Computer Graphics Forum (Proc. of EUROGRAPHICS 2014)* (2014).

A ANCHOR CONSTRAINT DERIVATIVES

Since any anchor constraint is acting on a given edge segment on a specific rod, we will omit the indices for the rod and segment for ease of notation unless necessary. Following from the anchor constraint energy defined in Equation 1, the corresponding entries of the Jacobian for the position term are given by

$$\begin{aligned}\frac{\partial r_{pos}}{\partial p_i} &= (1 - \beta)I, \\ \frac{\partial r_{pos}}{\partial p_{i+1}} &= \beta I, \\ \frac{\partial r_{pos}}{\partial p_a} &= -I,\end{aligned}$$

with I denoting the 3-by-3 identity matrix. The entries of the Jacobian corresponding to the anchor direction terms are

$$\begin{aligned}\frac{\partial r_{dir}}{\partial e} &= -\frac{(z^T t)m}{\|e\|}, \\ \frac{\partial r_{dir}}{\partial \theta} &= -z^T(-d_1 \sin(\theta) + d_2 \cos(\theta)), \\ \frac{\partial r_{dir}}{\partial m_a} &= \frac{z}{\|m_a\|},\end{aligned}$$

with

$$z = -\frac{m \times m_a}{\|m \times m_a\|} \times m,$$

where $e = p_{i+1} - p_i$ denotes the i -th edge segment vector and $t = e/\|e\|$ is its tangent. d_1 and d_2 denote the directors of the edge segment that, together with the angle θ , define the material direction $m = d_1 \cos(\theta) + d_2 \sin(\theta)$.

Finally, we need the entries for the Hessian. The second derivatives of the anchor position terms vanish. For the entries of the direction terms, we first need some preliminary computations:

$$\begin{aligned}\frac{\partial t}{\partial e} &= \frac{I}{\|e\|} - \frac{ee^T}{\|e\|^3}, \\ \frac{\partial m}{\partial e} &= -\frac{tm^T}{\|e\|}, \\ \frac{\partial m}{\partial \theta} &= -d_1 \sin(\theta) + d_2 \cos(\theta),\end{aligned}$$

$$\begin{aligned}\frac{\partial \|m \times m_a\|}{\partial e} &= -\frac{m \times m_a}{\|m \times m_a\|}^T [m_a]_{\times} \frac{\partial m}{\partial e}, \\ \frac{\partial \|m \times m_a\|}{\partial m_a} &= \frac{m \times m_a}{\|m \times m_a\|}^T [m]_{\times}, \\ \frac{\partial z}{\partial e} &= \frac{\frac{\partial m}{\partial e}(m^T m_a) + m(m_a^T \frac{\partial m}{\partial e}) - 2m_a(m \frac{\partial m}{\partial e})}{\|m \times m_a\|} \\ &\quad - \frac{m \times (m \times m_a) \frac{\partial \|m \times m_a\|}{\partial e}}{\|m \times m_a\| \|m \times m_a\|}, \\ \frac{\partial z}{\partial \theta} &= \left(-\frac{\frac{\partial m}{\partial \theta} \times m_a}{\|m \times m_a\|} + \frac{(m \times m_a) \frac{\partial \|m \times m_a\|}{\partial \theta} \frac{\partial m}{\partial \theta} \times m_a}{\|m \times m_a\| \|m \times m_a\|} \right) \times m \\ &\quad - \frac{m \times m_a}{\|m \times m_a\|} \times \frac{\partial m}{\partial \theta}, \\ \frac{\partial z}{\partial m_a} &= \frac{mm^T - I}{\|m \times m_a\|} - \frac{m \times (m \times m_a) \frac{\partial \|m \times m_a\|}{\partial m_a}}{\|m \times m_a\| \|m \times m_a\|},\end{aligned}$$

with $[m_a]_{\times}$ denoting the skew-symmetric matrix of the vector m_a . The entries of the Hessian are then given by

$$\begin{aligned}\frac{\partial^2 r_{dir}}{\partial e \partial e} &= -\frac{m(t^T \frac{\partial z}{\partial e} + z^T \frac{\partial t}{\partial e}) + (z^T t) \frac{\partial m_i}{\partial e}}{\|e\|} - \frac{(z^T t)(mt^T)}{\|e\| \|e\|}, \\ \frac{\partial^2 r_{dir}}{\partial e \partial \theta} &= -\frac{(\frac{\partial z}{\partial \theta} t)m - (z^T t) \frac{\partial m}{\partial \theta}}{\|e\|}, \\ \frac{\partial^2 r_{dir}}{\partial \theta \partial \theta} &= \frac{\partial z}{\partial \theta}^T \frac{\partial m}{\partial \theta} + z^T(-d_1 \cos(\theta) - d_2 \sin(\theta)), \\ \frac{\partial^2 r_{dir}}{\partial e \partial m_a} &= -\frac{m(t^T \frac{\partial z}{\partial m_a})}{\|e\|}, \\ \frac{\partial^2 r_{dir}}{\partial \theta \partial m_a} &= \frac{\partial m}{\partial \theta}^T \frac{\partial z}{\partial m_a}.\end{aligned}$$